Journal of
Translational Regenerative Medicine

2026. Volume 1

Research Paper

Development and Characterization of an Alpha-tricalcium Phosphate-based Calcium Phosphate Cement Prepared by Bioorthogonal Reactions

Marzie Moraveji[1], Nader Nezafati[1*], Mohammad Pazouki[2]

1. Biomaterials Group, Department of Nanotechnology and Advanced Materials, Materials and Energy Research Center, Karaj, Iran.
2. Department of Energy, Materials and Energy Research Center, Karaj, Iran.

Use your device to scan and read the article online

Citation Moraveji M, Nezafati N, Pazouki M. Development and Characterization of an Alpha-tricalcium Phosphate-based Calcium Phosphate Cement Prepared by Bioorthogonal Reactions. Journal of Translational Regenerative Medicine. 2025; 1:E1018. http://dx.doi.org/10.32598/JTRM.1.1018

http://dx.doi.org/10.32598/JTRM.1.1018

ABSTRACT

Background: A bioorthogonally modified calcium phosphate cement (CPC) was developed to enhance hydroxyapatite (HA) formation, porosity, and biological performance for bone tissue engineering applications.

Methods: The modification strategy was based on surface functionalization of α-tricalcium phosphate (α-TCP) powders with azide- and cyclooctyne-containing molecules to promote apatite nucleation and bioactivity.

Results: Structural characterization by X-ray diffraction (XRD) revealed enhanced HA formation in modified samples. The ratio of the HA peak to the α-TCP peak indicated accelerated HA formation. SEM observations revealed a transition from cauliflower-like and needle-like apatite morphologies in control samples (C-CPC) to plate-like HA morphologies in modified cements (M-CPC), resembling natural bone apatite. Porosity measurements showed a significant increase from nearly 43 for C-CPC to 71 for M-CPC. Despite the higher porosity, both groups exhibited similar biodegradation behavior over 28 days of immersion, with the pH decreasing only slightly from 7.2 to approximately 6.9. Mechanical evaluation indicated reduced compressive strength, Young's modulus, and energy absorption in M-CPC, which was attributed to increased porosity and changes in apatite morphology. Cytocompatibility assessment demonstrated cell viabilities, exceeding 90% in most conditions and remaining above 85% in all cases, satisfying ISO 10993-5 requirements. SEM analysis further confirmed favorable cell attachment and spreading on both cement surfaces.

Conclusion: The findings demonstrate that bioorthogonal modification of CPCs effectively enhances apatite formation, porosity, and biological performance while maintaining acceptable biocompatibility.

Keywords: Bioorthogonal reaction, Calcium phosphate cement (CPC), Hydroxyapatite (HA), Cytotoxicity, Cell attachment

Article info:
Received: 10 Mar 2026
Accepted: 25 Sep 2026
Publish: 10 Nov 2026

*** Corresponding Author:**
Nader Nezafati, Associate Professor.
Address: *Biomaterials Group, Department of Nanotechnology and Advanced Materials, Materials and Energy Research Center, Karaj, Iran.*
Phone: *+98 (26) 36280040*
E-Mail: *N.nezafati@Merc.ac.ir*

Highlights

- Bioorthogonal modification accelerated HA formation in the α-TCP-based CPC.
- HA/α-TCP peak ratio increased after immersion in SBF.
- The cement porosity significantly increased after modification.
- Plate-like HA morphology resembling natural bone apatite was obtained.
- Modified cement maintained excellent cytocompatibility with >85% cell viability.

Plain Language Summary

There are various types of bone cements based on calcium phosphates. In this study, a modified calcium phosphate cement (CPC) was developed using bioorthogonal reactions to enhance hydroxyapatite (HA) formation, porosity, and biological performance for bone tissue engineering applications. The modification strategy was based on surface functionalization of α-tricalcium phosphate (α-TCP) powders with azide- and cyclooctyne-containing molecules. The findings revealed that bioorthogonal modification of CPCs effectively enhances HA formation, porosity, and biological performance while maintaining acceptable biocompatibility.

Introduction

Nowadays, bone substitutes have attracted considerable attention in the field of biomaterials because of their ability to treat bone defects and improve bone function. They can be broadly categorized into natural (autografts, allografts, xenografts, and natural polymers) and synthetic (bone cements, hydroxyapatite (HA), tricalcium phosphate (TCP), bioactive glass, and polymers) materials [1, 2]. So far, various types of bone cements based on calcium phosphates [3], calcium sulfates [1], calcium silicates [4], acrylic resins [5], and/or their composites [6] have been studied. Acrylic cements (polymer-based cements) have even found clinical applications [7]. Among them, calcium phosphate cements (CPCs) have received considerable attention due to their similarity to the chemical composition of the mineral component of bone, as well as their bioactivity, biocompatibility, and biodegradability (depending on their composition and physical properties) [8]. In addition to these features, the microstructure of CPCs is also important. Macroporosity and microporosity are two major factors that significantly affect the physical and biological behaviors of CPCs. Macroporosity is perhaps the most important factor that comes to mind when discussing osteoconductivity and osteoinductivity in bone substitutes. However, recent studies have demonstrated the significant role of microporosity in bone regeneration as well [9, 10]. For example, Bohner et al. found that bone growth and mineralized tissue formation (including cells, calcium phosphate, and collagen) in β-TCP-based materials containing both microporosity and macroporosity are superior to those observed in β-TCP materials possessing only macroporosity [9].

In fact, microporosity plays an important role in osteoconductivity and osteogenicity because it increases the specific surface area, thereby enhancing protein adsorption and interaction with cells [11], promoting resorption [12] and enhancing capillary forces [13]. It is worth noting that micropore-induced capillary forces can draw cells into the pores by deforming cell morphology [13]. Interestingly, a micropore size equal to or larger than the cell size is not required for cell penetration into the pores [13]. There are various ways to create microporosity within CPCs, such as increasing the liquid-to-powder ratio [14], increasing powder particle size [14], altering the morphology of HA [14], and modifying the surface energy of the powders (through surface modification) [14]. However, surface modification of powders appears to provide synergistic benefits compared to those achieved through other microporosity-inducing approaches in CPCs.

In our previous work, surface modification of powders using click-chemistry reactants was successfully performed, resulting in accelerated HA nucleation and enhanced bioactivity [15]. In the present study, we aimed

to evaluate the effect of bioorthogonal reactions on the microstructure of α-TCP-based CPCs. Therefore, the microstructure and physicochemical properties of the modified CPCs, including cement morphology, phase composition, and particle size distribution, were characterized. In addition, setting time, porosity, biodegradability, mechanical properties, and cellular behavior were evaluated using appropriate analytical techniques and compared with those of unmodified CPCs used as the control group.

Materials and Methods

Cement preparation

For the preparation of α-TCP-based CPCs, two types of powders were considered: a control sample (C-CPC) and a modified specimen with a click-chemistry reactant (M-CPC). These powders were prepared as described in our previous work [15]. In brief, synthesis of C-CP powder was performed by solid-state reaction of α-TCP and tetracalcium phosphate (TTCP) [16, 17], which were mixed with dicalcium phosphate anhydrate (DCPA). M-CP powder was prepared by dispersing two identical portions of C-CPC in deionized (DI) water. Sample 1 was functionalized with 6-azido hexanoic acid, while Sample 2 was treated with dibenzocyclooctyne-amine. Following overnight incubation at room temperature, both samples were rinsed, centrifuged, and dried at 50 ˚C. After mixing and dispersing the samples in dimethylformamide, the mixture was incubated at −30 ˚C (overnight), 4 ˚C (1 h), and room temperature (5 days). The powder was then collected by rinsing, centrifuging three times with DI water, and drying at 50 ˚C. The solid phase of the cement was then mixed with a 6 wt% Na_2HPO_4 solution as the liquid phase, owing to its ability to facilitate the cement-setting reaction while maintaining desirable workability and stability of the cement paste. The powder-to-liquid ratio (P/L) was 3 g/mL. At this ratio, the consistency and workability of the cement were maintained.

Cement characterization

The particle size and particle size distribution of C-CPC and M-CPC powders were determined and compared using dynamic light scattering (DLS; 90 Plus Particle Sizer, Brookhaven Instruments, Holtsville, NY, USA) at a wavelength of 532 nm and a temperature of 25 ˚C. The samples were prepared by dispersing a small amount of powder in water, followed by sonication for 10 min.

Phase analysis of the cements before and after soaking in simulated body fluid (SBF) was carried out using a Philips PW3710 X-ray diffractometer with Cu Kα radiation. The instrument was operated at 40 kV and 30 mA. The data were collected over the range of $20^\circ \leq 2\theta \leq 40^\circ$ at a scan rate of $2^\circ min^{-1}$.

The morphology of the samples before and after SBF immersion, as well as cell morphology, was examined using scanning electron microscopy (SEM; VEGA3 SBU, Tescan, USA). The compressive strength of the cements was measured using a universal testing machine (STM-120, Santam Co.) at a loading rate of 0.5 mm/min. For this purpose, cylindrical specimens were prepared in silicone molds measuring 12 mm in height and 6 mm in diameter. The initial setting time (IST) and final setting time (FST) of the C-CPC and M-CPC samples were determined using the Gillmore needle test (ASTM C266-89).

The porosity of the disc-shaped C-CPC and M-CPC samples was measured using the Archimedes immersion method. In this method, the samples were placed separately in boiling water for 2 h. After the boiling period, heating was discontinued, and the samples were left immersed in the water for an additional 24 h. The porosity was calculated using Equation 1:

$$1.\ P(\%) = \frac{\text{Saturated weight-Dry weight}}{\text{Saturated weight-Suspended wight}}$$

Acellular biomineralization of the cements

The C-CPC and M-CPC samples were individually soaked in containers containing 45 mL of SBF. The SBF solution was refreshed every 2 days. After 14 days, the four samples were dried at room temperature. The SBF solution was prepared according to the protocol described by Kokubo et al. [16] by dissolving NaCl (8.035 g/L), KCl (0.225 g/L), $K_2HPO_4 \cdot 3H_2O$ (0.231 g/L), $MgCl_2 \cdot 6H_2O$ (0.311 g/L), $CaCl_2$ (0.292 g/L), $NaHCO_3$(0.355 g/L), and Na_2SO_3 (0.072 g/L) in distilled water. The solution was buffered to pH 7.25 using 6.118 g/L tris (hydroxymethyl) aminomethane and 1 N HCl at 37 ˚C. Finally, phase analysis and morphological characterization were performed using X-ray diffraction (XRD) and SEM analyses, respectively. The biodegradability test was performed by soaking disc-shaped C-CPC and M-CPC cements in SBF for 28 days. The weights of the samples were measured on days 0, 3, 7, 14, 21, and 28. For weight measurement, the samples were completely dried in an oven at 50 ˚C.

Cellular evaluation of the cements

To evaluate the cytotoxicity of the cements, the MTT assay was used. For this purpose, 24-h and 48-h cement extracts were prepared in accordance with ISO 10993-5 guidelines. According to these guidelines, 1 mL of dulbecco's modified eagle medium (DMEM) containing 10% (v/v) fetal bovine serum (FBS) per 0.05 g of sample was used. Before the extraction procedure, each sample was sterilized by UV irradiation for 1 h and rinsed three times with phosphate buffered saline (1× PBS).

For the MTT assay, 10,000 human fibroblast (HFFF2) cells were seeded in a 96-well plate. After 24 h, the cell culture medium was replaced with the cement extract. The cells were exposed to the extracts for 24, 48, and 72 h. The control group was incubated in DMEM containing 10% (v/v) FBS. After the treatment period, the culture medium was discarded, the samples were rinsed with 1× PBS, and the cells (n=5 per group) were incubated with 100 µL of MTT solution (0.5 mg MTT/mL PBS) for 4 h. Finally, the MTT solution was removed, and the violet formazan crystals were dissolved in 100 µL of isopropanol for 20 min. The optical density (OD) of the dissolved formazan was measured using an ELISA microplate reader at wavelengths of 545 and 630 nm.

Cell attachment in the C-CPC and M-CPC cements was investigated by seeding 100,000 human fibroblast cells onto the sample surfaces. After 72 h, the samples were fixed with 4% (v/v) glutaraldehyde for 4 h at 4 ˚C, rinsed with 1× PBS, and dehydrated through a graded ethanol series (30%, 50%, 70%, and 95% ethanol).

Statistical analysis

All experiments were performed in triplicate (n=3) unless otherwise stated, and the results were presented as Mean±SD. Statistical analyses were performed in GraphPad Prism software version 10.2.2 (GraphPad Software, USA). Differences between C-CPC and M-CPC samples were evaluated using a student's t-test. For datasets involving multiple experimental factors or time points, two-way analysis of variance (ANOVA) followed by Tukey's post hoc test was applied.

Results

DLS analysis

The results of DLS analysis for the C-CPC powder revealed d_{50} values of approximately 6 µm for α-TCP, 13 µm for TTCP, and 2 µm for DCPA. According to the rule of mixtures, the mean particle size of the C-CPC powder mixture was approximately 6.98 µm. The DLS analysis of the M-CPC powder yielded a d_{50} of approximately 23 µm. The increase in the mean particle size from 6.98 µm to 23 µm indicates enhanced interparticle connectivity among the powders modified with azide and cycloalkyne reactants through click chemistry, leading to the formation of triazole rings (Table 1).

The particle size of the powders is one of the key factors influencing the properties of the cement.

Setting time test

Figure 1 plots the comparison of the IST and FST values for M-CPC and C-CPC samples. The modification of the powders increased the IST compared to the control sample (18±2.12 min vs 15±1.7 min) and the FST (35±3.12 min vs 27±1.2 min).

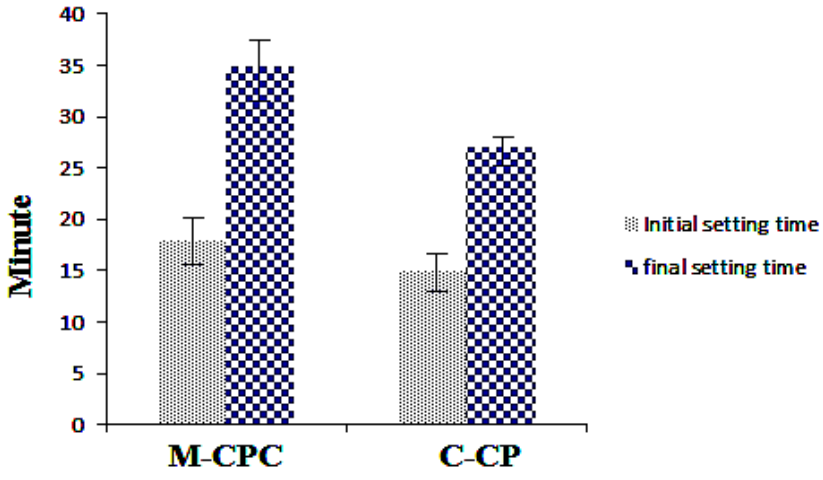

Figure 1. Initial and FSTs of the C-CPC and M-CPC samples, assessed using the Gillmore needle test

Table 1. Particle size characteristics of the cement powders determined by DLS analysis

Sample / Powder	Median Particle Size (d50)
α-TCP	~6
TTCP	~13
DCPA	~2
C-CPC powder	6.98
M-CPC powder	~23

Discussion

One reason for this observation may be the increase in particle size (according to the DLS results) and the corresponding decrease in specific surface area, which requires more time for the surface dissolution of the powders (the first step in the cement-setting process) and consequently increases the setting time. Another possible reason is the formation of HA on the surface of the modified powders during the modification process, as described in our previous study [15]. In summary, the presence of functional groups in the structures of azide and cyclooctyne molecules can accelerate HA nucleation and growth.

Indeed, the presence of carbonyl and amine groups in DBCO-amine [18] facilitates the adsorption of Ca^{2+} and PO_4^{3-} ions, respectively, onto the powder surfaces. In addition, the carboxylic acid group of 6-azidohexanoic acid provides another potential binding site for Ca^{2+} ions. Furthermore, the triazole ring, which contains three nitrogen atoms, exhibits relatively high electron density, promoting interactions with Ca^{2+} ions. As a result, the formation of a low-solubility HA layer on the surface of the M-CPC powders may reduce their dissolution rate, which in turn could contribute to the prolonged setting time observed for M-CPC.

XRD analysis

Figure 2 shows the XRD patterns of C-CPC, C-CPC.SBF, M-CPC, and M-CPC.SBF. The three characteristic peaks of HA in the 2θ range of 31–33° can be clearly observed for M-CPC.SBF (JCPDS card No. 09-0432). In C-CPC and C-CPC.SBF samples, the α-TCP peak at approximately 30.7° was observed. In addition, the peak at approximately 22.8°, which is attributed to α-TCP, was present in all four samples.

It has been reported that the intensity ratio of the most intense HA peak (approximately 32°) to the most intense α-TCP peak (approximately 30.8°) can provide an approximate estimation of the HA/α-TCP phase ratio. However, the α-TCP peak at 30.8° was not clearly detectable in all samples. Therefore, the common α-TCP peak at 22.8° was selected as a reference peak to obtain semi-quantitative information regarding the HA/α-TCP ratio. The ratio of the peak height at approximately 32° to that at approximately 22.8° was 5.4, 5.7, 7.8, and 9.5 for C-CPC, C-CPC.SBF, M-CPC, and M-CPC.SBF, respectively.

SEM analysis

SEM micrographs of C-CPC, C-CPC.SBF, M-CPC, and M-CPC.SBF are presented in Figure 3. As shown in the figure, HA formed on the surface of C-CPC with a cauliflower-like morphology (Figure 3a), whereas C-CPC.SBF exhibited a needle-like HA morphology on its surface (Figure 3b). In contrast, M-CPC and M-CPC.SBF exhibited a plate-like morphology of HA on their surfaces (Figures 3c and 3d). Since biological bone apatite typically exhibits a plate-like morphology, the formation of plate-like HA on the surface of M-CPC may be considered a biomimetic feature and a potential advantage of the modification process.

Effect of modification on the porosity and biodegradability

The porosity percentages of C-CPC and M-CPC cements were 43.24±1.62% and 70.71±2.05%, respectively (Figure 4a). This result demonstrates a significant increase in porosity for M-CPC than for C-CPC. One possible explanation for this observation is the larger particle size of the modified powders (23 μm) compared to that of the control powders (6.98 μm). It has been reported that an increase in particle size can lead to larger pore sizes and a higher overall porosity level. Another possible reason may be the differences in HA

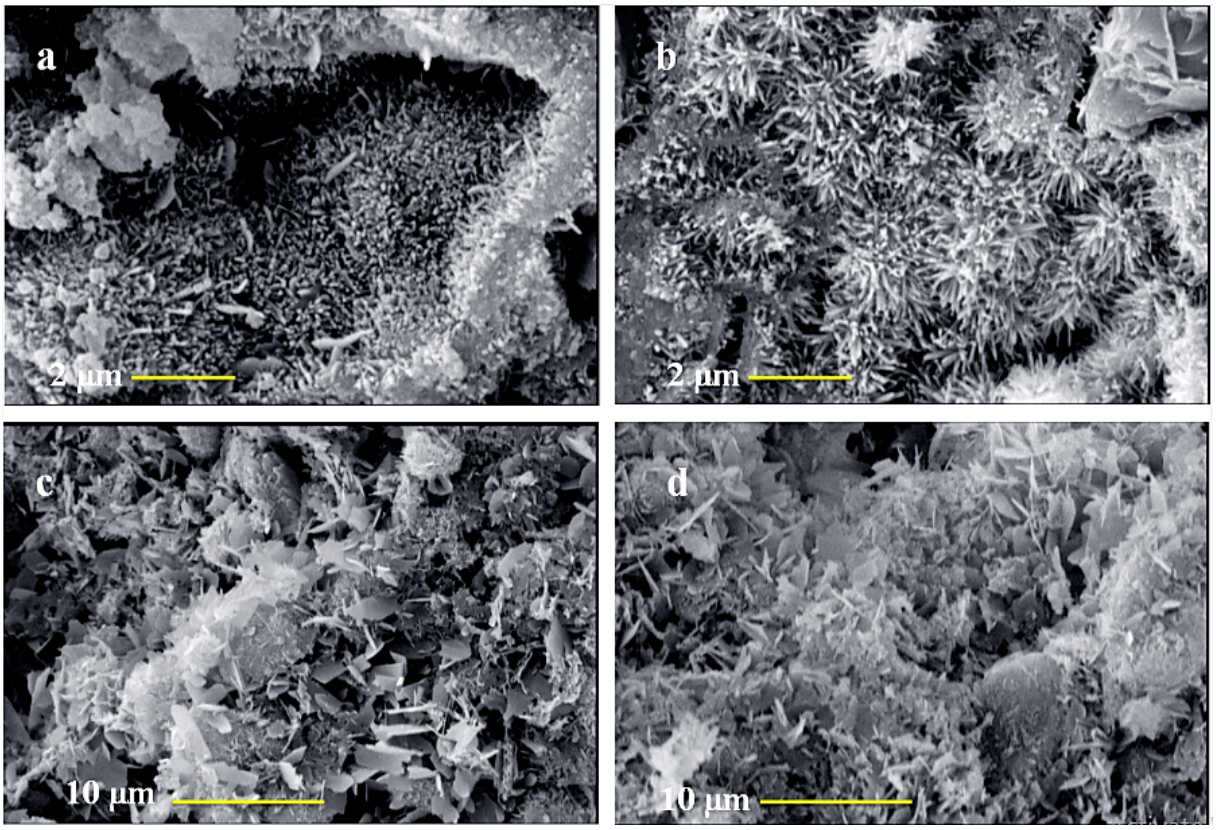

Figure 2. The XRD patterns of C-CPC, C-CPC.SBF (control cement immersed in SBF), M-CPC, and M-CPC.SBF (modified cement immersed in SBF)

morphology between M-CPC and C-CPC. According to recent studies, plate-like HA particles often exhibit a less efficient packing arrangement than needle-like particles, which can contribute to increased porosity [19, 20].

The biodegradability results showed no significant change in the weight of either the C-CPC or M-CPC samples during the 28-day immersion period (Figure 4b). In addition, the pH of the SBF solution decreased from approximately 7.2 on day 1 to around 6.9 on day

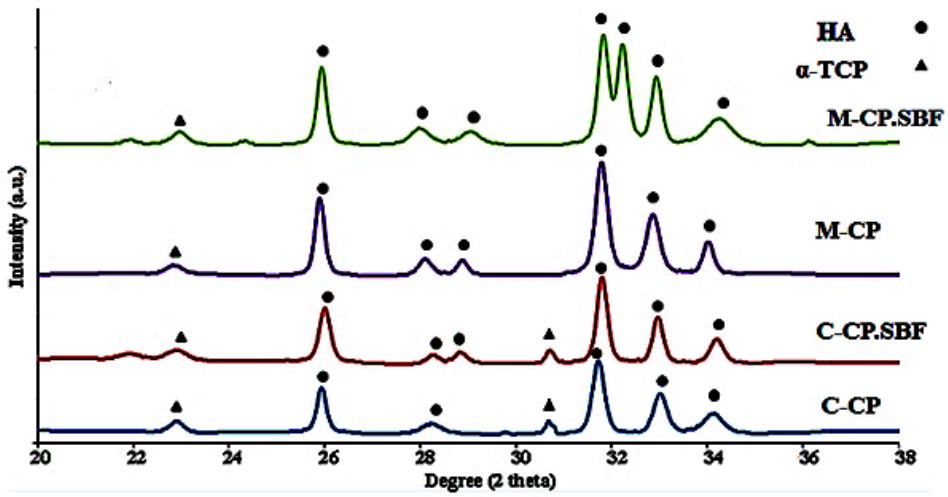

Figure 3. The SEM micrographs showing the surface morphology of (a) C-CPC, (b) C-CPC.SBF, (c) M-CPC, and (d) M-CPC.SBF

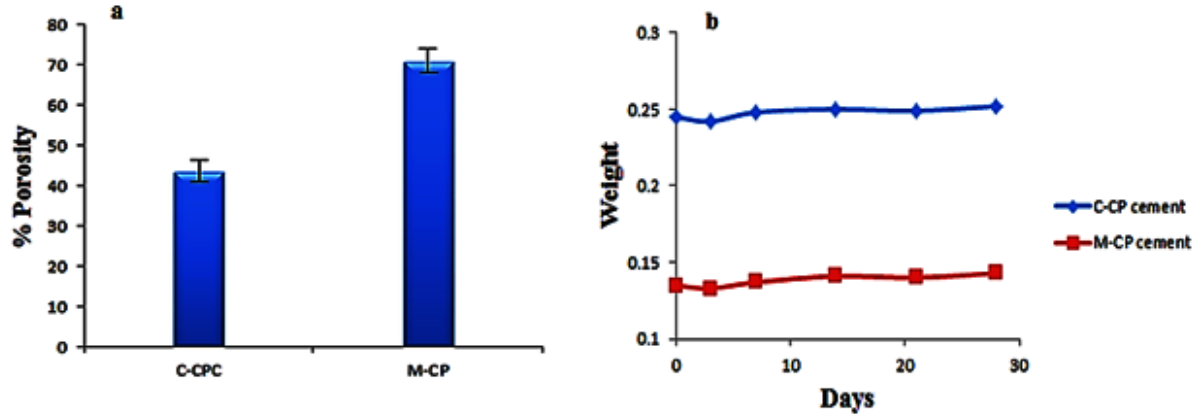

Figure 4. Porosity (a) and biodegradability (b) of C-CPC and M-CPC

28. Given the higher porosity of M-CPC compared to C-CPC, a greater weight loss was expected for M-CPC. However, the results showed that both samples exhibited approximately similar weight losses. One possible explanation for this observation is accelerated HA nucleation and enhanced conversion of α-TCP to HA in the modified cement. Although increased porosity generally promotes degradation, enhanced HA formation may reduce material dissolution due to the relatively low solubility of HA. Therefore, the opposing effects of increased porosity and accelerated HA formation may have compensated for each other, resulting in comparable biodegradation behavior for the two cement formulations.

Mechanical properties

The study of the effect of powder modification on the mechanical properties of the cement revealed a decrease in compressive strength (Figure 5a), energy absorption up to the failure point (Figure 5b), and Young's modulus (Figure 5c). Two possible explanations can be mentioned for these observations. First, the reduction in mechanical properties may be related to the higher porosity of M-CPC, which resulted from the increased particle size of the modified powders compared to the control powders. Increased porosity is known to reduce the effective load-bearing area and act as stress concentration sites within the cement matrix. Second, the decrease in mechanical performance may be due to differences in HA morphology between M-CPC and C-CPC, arising from differences in the surface energy of the powders. Plate-like HA structures may provide lower mechanical reinforcement than needle-like HA crystals, resulting in reduced mechanical properties.

SEM images of the fracture surfaces revealed a more porous microstructure in M-CPC and a denser, more compact microstructure in C-CPC (Figure 6). Furthermore, longer cracks were observed in M-CPC, whereas shorter cracks were present in C-CPC. This observation suggests that crack propagation occurred more readily in M-CPC, thereby reducing its resistance to fracture and energy absorption capacity.

The reduction in compressive strength, Young's modulus, and energy absorption observed in the modified cement is consistent with previous reports on porous CPCs. Ambard et al. [8] emphasized that mechanical performance is strongly influenced by porosity, with increasing pore volume generally leading to reduced load-bearing capacity and increased stress concentration. Similarly, Grosfeld et al. [3] demonstrated that introducing porosity into injectable CPC systems improved biological performance at the expense of mechanical strength.

The fracture surface morphology observed in the present study, characterized by longer crack propagation paths in the modified cement, further supports the role of increased porosity in reducing mechanical integrity. Therefore, the observed reduction in mechanical properties may be regarded as an expected trade-off associated with the development of a more biologically favorable microstructure.

Cell study: MTT assay and cell adhesion

MTT assay results for 24, 48, and 72 h of cell exposure to 24-h and 48-h extracts of M-CPC and C-CPC are presented in Figure 7. Cell viability across all groups exceeded 90%, except for two conditions: cells treated with the 24-h M-CPC extract for 48 h and cells treated with the 48-h M-CPC extract for 72 h, in which viability remained above 85%. According to ISO 10993-5, a biomaterial is considered non-cytotoxic and biocompatible

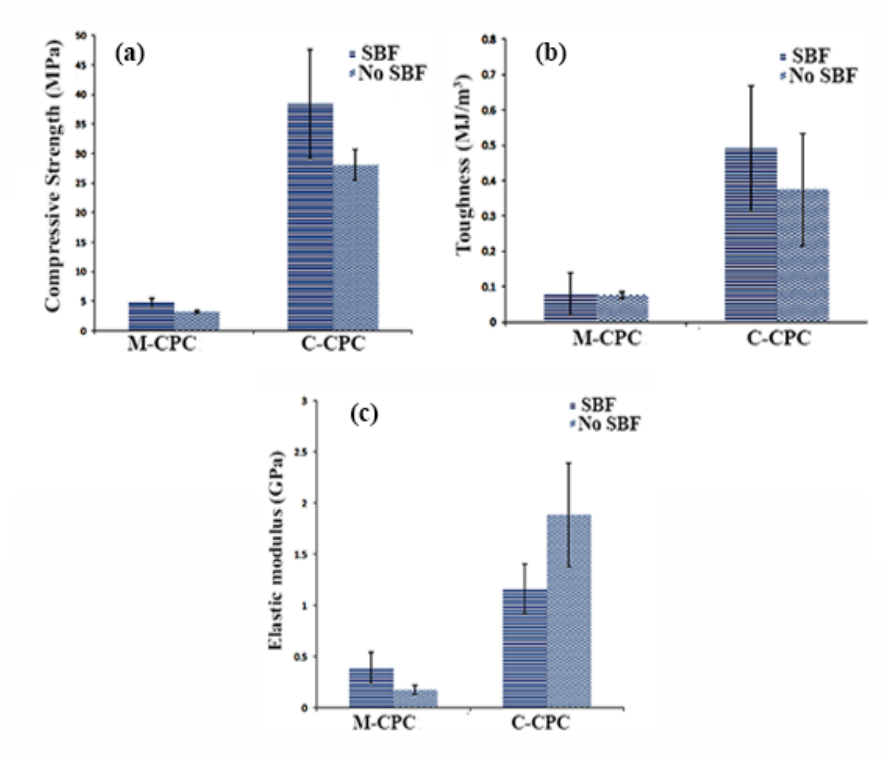

Figure 5. Mechanical properties of C-CPC and M-CPC

a) Compressive strength, b) energy absorption up to the failure point, c) Young's modulus measured under uniaxial compression

if cell viability exceeds 70%. Therefore, both M-CPC and C-CPC can be classified as biocompatible biomaterials.

SEM images of cell adhesion in M-CPC and C-CPC after 72 h of culture are shown in Figure 8. The SEM micrographs demonstrate good cell attachment on both cement types. In M-CPC, in addition to well-spread cells, cells with a more rounded morphology were observed. Previous studies have shown that several factors, including surface roughness, chemical composition, surface functional groups, zeta potential, and microstructure, can influence cell morphology. Indeed, zeta potential is strongly influenced by surface functional groups. It has been reported that different cell types exhibit different responses to surface charge. Some cells preferentially adhere to positively charged surfaces (e.g. NH_2-modified surfaces), whereas others show a preference for negatively charged surfaces (e.g. COOH-modified surfaces).

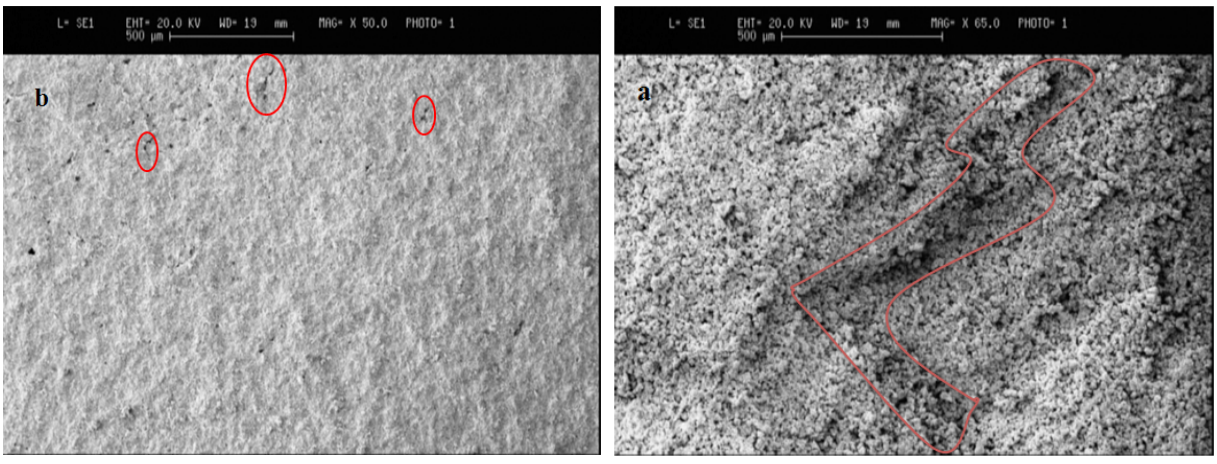

Figure 6. The SEM images of fracture surfaces after compressive testing

a) C-CPC, b) M-CPC

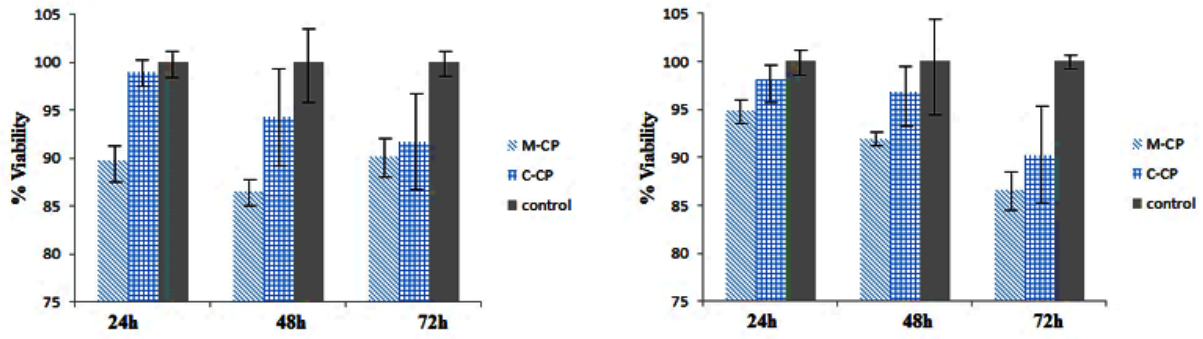

Figure 7. Cell viability of human fibroblast cells exposed to extracts obtained from C-CPC and M-CPC for different incubation periods

a) 24-h extracts, b) 48-h extracts

Microporosity is another important microstructural parameter. Previous studies have suggested that when the capillary force generated by micropores approaches the critical force required for cell deformation, cells cultured on microporous surfaces tend to deform and penetrate into the pores. According to our previous study, the zeta potential of C-CPC was approximately −18 mV, whereas surface modification increased it to approximately −40 to −50 mV. However, this change did not appear to significantly affect cell attachment or overall cell morphology. Therefore, microporosity may be the dominant factor influencing cell morphology in the present study. Specifically, the higher porosity of M-CPC may generate stronger capillary forces, thereby promoting cell deformation and infiltration into the microporous structure.

Biological evaluation demonstrated excellent cytocompatibility for both cement formulations, with cell viability consistently exceeding the threshold specified by ISO 10993-5. These findings are in agreement with the results of previous studies reporting favorable cellular responses to calcium phosphate ceramics and cements. Samavedi et al. [11] highlighted that calcium phosphate materials generally support cell attachment and proliferation due to their chemical similarity to bone mineral. Furthermore, Polak et al. [13] demonstrated that microporous substrates can enhance cellular infiltration through capillary-force-driven mechanisms. The presence of well-spread cells on both cement surfaces and the observation of altered cell morphology in the modified cement suggest that the increased microporosity generated by bioorthogonal modification may facilitate more intimate cell–material interactions. Importantly, the substantial change in surface chemistry and zeta potential resulting from modification did not induce any detectable cytotoxic effects, further confirming the biological safety of the proposed approach.

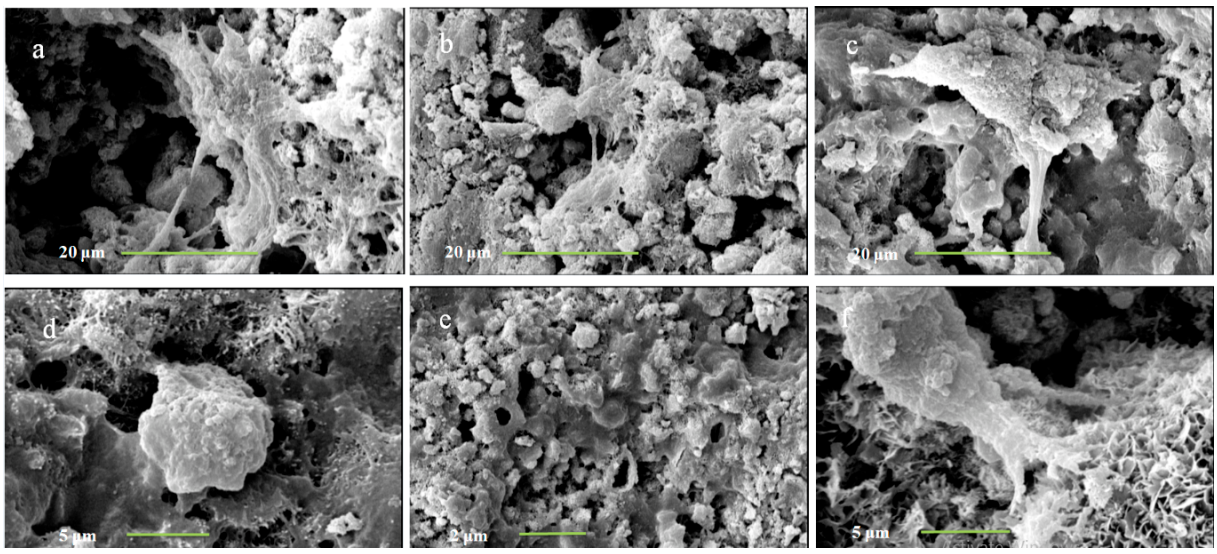

Figure 8. SEM micrographs showing the attachment and morphology of human fibroblast cells on the surfaces of C-CPC (a, b, c) and M-CPC (d, e, f) for 72 h

Conclusion

Bioorthogonal surface modification of α-TCP-based CPC effectively improved its bioactivity and microstructural characteristics. The modified cement exhibited enhanced HA formation, as evidenced by the increase in the HA/α-TCP peak ratio from 5.4 in the control cement to 7.8 in the modified cement and further to 9.5 after immersion in SBF. In addition, surface modification significantly increased cement porosity, resulting in a microstructure that may be more favorable for tissue ingrowth and cell–material interactions. SEM observations revealed the formation of plate-like HA crystals in the modified cement, a morphology that more closely resembles that of the mineral phase in natural bone. This biomimetic morphology may contribute to improved biological performance and osteogenic potential. Although the increase in porosity resulted in reductions in compressive strength, energy absorption, and Young's modulus, the modified cement maintained sufficient structural integrity for potential bone tissue engineering applications. Despite its higher porosity, the modified cement exhibited biodegradation behavior comparable to that of the control cement over the 28-day evaluation period, suggesting that the enhanced HA formation may compensate for the increased susceptibility to degradation. Furthermore, biological evaluation demonstrated excellent cytocompatibility, with cell viability consistently exceeding 85% and generally remaining above 90%. SEM analysis also confirmed favorable cell attachment and spreading on both cement formulations.

Overall, the results suggest that bioorthogonal surface modification is a promising approach for tailoring the microstructure and biological performance of CPCs. The combination of enhanced bioactivity, increased porosity, biomimetic HA morphology, and excellent cytocompatibility highlights the potential of the modified cement for future bone regeneration and tissue engineering applications.

Ethical Considerations

Compliance with ethical guidelines

There were no ethical considerations to be considered in this research.

Funding

This study was financially supported by the Materials and Energy Research Center (MERC) (Grant No.: 241149602).

Authors' contributions

Conceptualization: Nader Nezafati; Methodology: Marzie Moraveji and Nader Nezafati; Data interpretation, Characterization work and writing the original draft: Marzie Moraveji; Resources review and editing: All authors; Project administration: Mohammad Pazouki and Nader Nezafati; Supervision: Mohammad Pazouki.

Conflict of interest

The authors declared no conflict of interest.

Acknowledgments

The authors would like to acknowledge the Materials and Energy Research Center (MERC) for its experimental laboratories in performing this research work.

References

[1] Cho JH, Song HK. Current concepts and applications of bone graft substitutes in orthopedic surgery. Journal of Musculoskeletal Trauma. 2025; 38(4):169-77. [DOI:10.12671/jmt.2025.00248]

[2] Fernandez de Grado G, Keller L, Idoux-Gillet Y, Wagner Q, Musset AM, Benkirane-Jessel N, et al. Bone substitutes: A review of their characteristics, clinical use, and perspectives for large bone defects management. Journal of Tissue Engineering. 2018; 9:2041731418776819. [DOI:10.1177/2041731418776819] [PMID] [PMCID]

[3] Grosfeld EC, Smith BT, Santoro M, Lodoso-Torrecilla I, Jansen JA, Ulrich DJ, et al. Fast dissolving glucose porogens for early calcium phosphate cement degradation and bone regeneration. Biomedical Materials. 2020; 15(2):025002. [DOI:10.1088/1748-605X/ab5f9c] [PMID] [PMCID]

[4] Wickramasinghe ML, Dias GJ, Premadasa KMGP. A novel classification of bone graft materials. Journal of Biomedical Materials Research. Part B, Applied Biomaterials. 2022; 110(7):1724-49. [DOI:10.1002/jbm.b.35029] [PMID]

[5] Kehribar L, Aydın M, Coşkun HS, Surucu S. Silver nanoparticles enhance the antibacterial effect of antibiotic-loaded bone cement. Cureus. 2023; 15(2):e34992. [DOI:10.7759/cureus.34992] [PMID] [PMCID]

[6] Matos AC, Marques CF, Pinto RV, Ribeiro IA, Gonçalves LM, Vaz MA, et al. Novel doped calcium phosphate-PMMA bone cement composites as levofloxacin delivery systems. International Journal of Pharmaceutics. 2015; 490 (1-2):200-8. [DOI:10.1016/j.ijpharm.2015.05.038] [PMID]

[7] Restucci-Orozco JP, Muñoz-Velez MF, Arteaga-Pedraza NA, Grande-Tovar CD, Valencia-Llano CH, Mina-Hernandez JH. A review of acrylic bone cement in the Masquelet technique: From temporary spacer to a bioactive modulator of the induced membrane. Sci. 2026; 8(6):125. [DOI:10.3390/sci8060125]

[8] Ambard AJ, Mueninghoff L. Calcium phosphate cement: Review of mechanical and biological properties. Journal of Prosthodontics: Official Journal of the American College of Prosthodontists. 2006; 15(5):321-8. [DOI:10.1111/j.1532-849X.2006.00129.x] [PMID]

[9] Bohner M, Baroud G, Bernstein A, Döbelin N, Galea L, Hesse B, et al. Characterization and distribution of mechanically competent mineralized tissue in micropores of β-tricalcium phosphate bone substitutes. Materials Today. 2017; 20(3):106-15. [DOI:10.1016/j.mattod.2017.02.002]

[10] Grewal NS, Verma M, Kumar S, Khan AR, Kumar K, Sharma N. Advances in growth factor-containing 3D printed scaffolds in orthopedics. Journal of Magnesium and Alloys. 2026; 16:102010. [DOI: 10.1016/j.jma.2026.102010]

[11] Samavedi S, Whittington AR, Goldstein AS. Calcium phosphate ceramics in bone tissue engineering: A review of properties and their influence on cell behavior. Acta Biomaterialia. 2013; 9(9):8037-45. [DOI:10.1016/j.actbio.2013.06.014] [PMID]

[12] Lapczyna H, Galea L, Wüst S, Bohner M, Jerban S, Sweedy A, et al. Effect of grain size and microporosity on the in vivo behaviour of β-tricalcium phosphate scaffolds. European Cells & Materials. 2014; 28:299-319. [DOI:10.22203/eCM.v028a21] [PMID]

[13] Polak SJ, Rustom LE, Genin GM, Talcott M, Wagoner Johnson AJ. A mechanism for effective cell-seeding in rigid, microporous substrates. Acta Biomaterialia. 2013; 9(8):7977-86. [DOI:10.1016/j.actbio.2013.04.040] [PMID] [PMCID]

[14] Dorozhkin SV. Self-setting calcium orthophosphate formulations. Journal of Functional Biomaterials. 2013; 4(4):209-311. [DOI:10.3390/jfb4040209] [PMID] [PMCID]

[15] Moraveji M, Nezafati N, Pazouki M, Hesaraki S. Bioorthogonal surface modified α-TCP-based bone filler for enhancement of apatite formation and bioactivity. Ceram Int. 2019; 45(5):5981-6. [DOI:10.1016/j.ceramint.2018.12.068]

[16] Kokubo T, Takadama H. How useful is SBF in predicting in vivo bone bioactivity? Biomaterials. 2006; 27(15):2907-15. [DOI:10.1016/j.biomaterials.2006.01.017] [PMID] [PMCID]

[17] Carrodeguas RG, De Aza S. α-Tricalcium phosphate: Synthesis, properties and biomedical applications. Acta Biomaterialia. 2011; 7(10):3536-46. [DOI:10.1016/j.actbio.2011.06.019] [PMID]

[18] Lang K, Chin JW. Bioorthogonal reactions for labeling proteins. ACS Chemical Biology. 2014; 9(1):16-20. [DOI:10.1021/cb4009292] [PMID]

[19] Viswanath B, Ravishankar N. Controlled synthesis of plate-shaped hydroxyapatite and implications for the morphology of the apatite phase in bone. Biomaterials. 2008; 29(36):4855-63. [DOI:10.1016/j.biomaterials.2008.09.001] [PMID]

[20] Neira IS, Kolen'ko YV, Lebedev OI, Van Tendeloo G, Gupta HS, Guitián F, et al. An effective morphology control of hydroxyapatite crystals via hydrothermal synthesis. Crystal Growth and Design. 2009; 9(1):466-74. [DOI:10.1021/cg800738a]